Unraveling the interlayer-related phonon self-energy renormalization in bilayer graphene

SCIENTIFIC REPORTS

OPEN

SUBJECT AREAS:
OPTICAL PROPERTIES AND DEVICES
ELECTRONIC PROPERTIES AND DEVICES
SEMICONDUCTORS
NANOSCALE DEVICES

Received
6 September 2012

Accepted
26 November 2012

Published
21 December 2012

Correspondence and requests for materials should be addressed to P.T.A. (ptaraujo@mit.edu)

Unraveling the interlayer-related phonon self-energy renormalization in bilayer graphene

Paulo T. Araujo[1], Daniela L. Mafra[1,2], Kentaro Sato[3], Riichiro Saito[3], Jing Kong[1] & Mildred S. Dresselhaus[1,4]

[1]Department of Electrical Engineering and Computer Sciences, Massachusetts Institute of Technology, Cambridge, MA 02139-4307, USA, [2]Departamento de Física, Universidade Federal de Minas Gerais, Belo Horizonte, MG, 30123-970 Brazil, [3]Department of Physics, Tohoku University, Sendai 980-8578, Japan, [4]Department of Physics, Massachusetts Institute of Technology, Cambridge, MA 02139-4307, USA.

In this letter, we present a step towards understanding the bilayer graphene (2LG) interlayer (IL)-related phonon combination modes and overtones as well as their phonon self-energy renormalizations by using both gate-modulated and laser-energy dependent inelastic scattering spectroscopy. We show that although the IL interactions are weak, their respective phonon renormalization response is significant. Particularly special, the IL interactions are mediated by Van der Waals forces and are fundamental for understanding low-energy phenomena such as transport and infrared optics. Our approach opens up a new route to understanding fundamental properties of IL interactions which can be extended to any graphene-like material, such as MoS_2, WSe_2, oxides and hydroxides. Furthermore, we report a previously elusive crossing between IL-related phonon combination modes in 2LG, which might have important technological applications.

In spite of its outstanding properties, for many practical purposes, that, for example, require a band gap, single layer graphene (1LG) cannot be readily applied without the use of complex engineering procedures[1–5]. One possible and interesting solution that responds constructively to several drawbacks of 1LG is to look at its multilayer graphene (MLG) counterparts[1–5]. MLG systems involve weak interlayer (IL) interactions mediated by Van-der-Waals (VdW) forces. These IL interactions are sensitive to the number of layers and stacking order and are important for technological applications of these systems because they are important for the low-energy electronic and vibrational properties and, therefore, will be important for phenomena such as transport, infrared optics and telecommunication bands in the infrared (IR) range[6–8]. In bilayer graphene (2LG), although the effects of the IL interactions on the electronic properties are well understood[9,10], the present understanding of IL-related vibrational properties, electron-electron (e-e), phonon-phonon (ph-ph), and electron-phonon (e-ph) interactions is still under development[11–15].

As regards the IL vibrational properties in 2LG, C. H. Lui *et al.*[8] studied the out-of-plane optical (ZO′) phonon mode (with frequency $\omega_{ZO'} = 90$ cm^{-1} predicted at the Γ-point, as shown in Fig. 1b). The ZO′ mode is also known as the IL breathing mode-LBM, and its combination mode LOZO′ with the longitudinal optical (LO) phonon (with frequency $\omega_{LO} = 1575$ cm^{-1} predicted at the Γ-point, as shown in Fig. 1b) occurs in the range for $\omega_{LOZO'}$ from 1600 to 1800 cm^{-1}, for MLG with up to 6 layers, thereby explaining their frequency dependence on both the number of layers and their stacking orders[8]. The other related LOZA combination mode (ZA is the IL out-of-plane acoustic mode whose frequency ω_{ZA} is zero at the Γ-point, as shown in Fig. 1b, and the 2ZO overtone (ZO is the out-of-plane tangential optical mode with frequency $\omega_{ZO} = 885$ cm^{-1} predicted at the Γ-point, as shown in Fig. 1b) demand a more detailed analysis, which is still elusive. All these features involve $q \neq 0$ (throughout the text, q is the phonon wave-vector) intravalley (AV) processes, therefore occurring around the Γ-point in the Brillouin zone. However, only the 2ZO overtone presents two possible forward ($q \approx 0$) and backward ($q \approx 2k$) scattering mechanisms[11]. Note that both the ZA and ZO modes are not Raman active at the Γ-point, where $q = 0$. In spite of recent advances in the study of these interlayer modes, their phonon self-energies and e-ph interactions for these IL-dependent modes have hardly been discussed. It is worth saying that, these modes ranging from 1600 to 1800 cm^{-1} are spectroscopic signatures for MLG and by understanding them in detail, we can understand the VdW-related phonon-dependent phenomena associated with these systems. Such knowledge

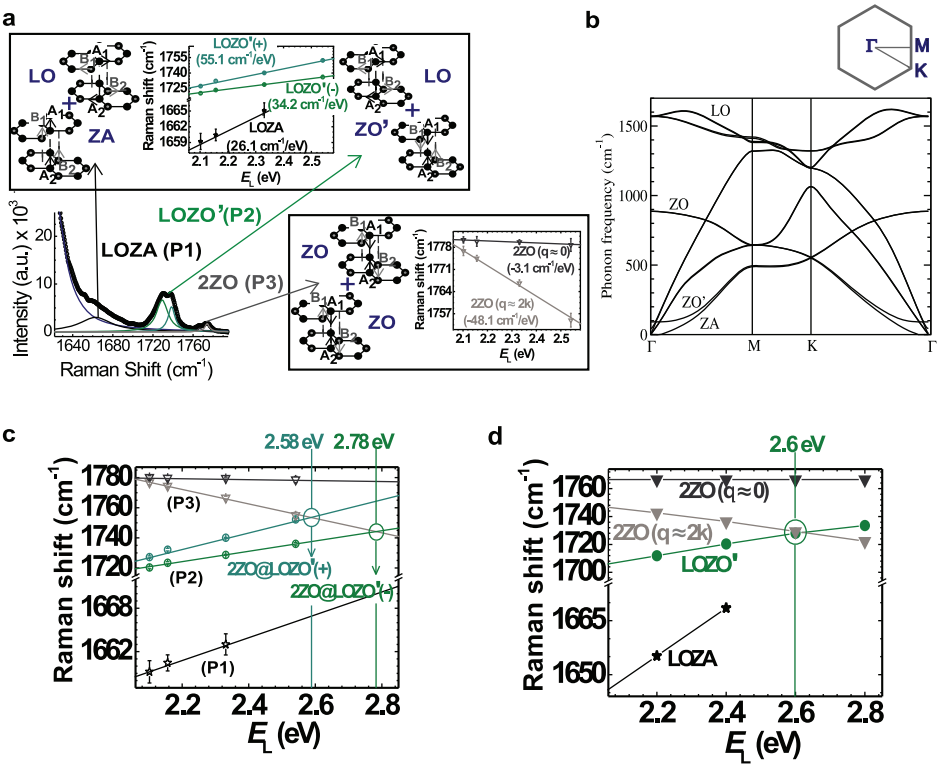

Figure 1 | Interlayer-related combination of phonon modes and overtones. (a) LOZA (P1) and LOZO′ (P2) combination modes and the 2ZO (P3) overtone as they appear in the Raman spectra taken with the 532 nm laser line. The solid lines are Lorentzian curves used to fit the spectrum. The upper and lower boxes show the lattice vibrations associated with each normal mode involved in the combination modes and overtones and their frequency dispersion as a function of E_L as shown in (c). (b) The calculated 2LG phonon dispersion showing the LO phonon mode (1575 cm^{-1} at the **Γ**-point), the ZO phonon mode (885 cm^{-1} at the **Γ**-point), the ZO′ phonon mode (90 cm^{-1} at the **Γ**-point) and the ZA phonon mode (0 cm^{-1} at the **Γ**-point)[11]. The inset shows the 2LG first Brillouin zone with the high-symmetry points **Γ**, **M** and **K**. (c) The Raman shift as a function of E_L, showing that the LOZO′ (P2) combination mode will be crossed by the 2ZO $q \approx 2k$ overtone at 2.58 eV and, according to the dispersion obtained in this work, will likely be crossed again at 2.78 eV. The symbols correspond to the experimental data. The solid lines are the fitting curve results. (d) The full symbols and solid lines are the theoretical frequency dispersion prediction for the LOZA (stars), LOZO′ (circles) and 2ZO overtones (down triangles) with a cross point at 2.6 eV between the 2ZO $q \approx 2k$ and the LOZO′ modes.

will have considerable impact on developing this research field, by opening a route to understanding IL interactions in similar, but more complex 2D-layered materials, such as MoS_2, WSe_2, oxides and hydroxides.

In the present letter we use gate-modulated and laser-energy (E_L)-dependent resonant Raman spectroscopy (RRS) together to address two fundamental issues regarding IL-interactions in 2LG systems: (1) we discuss in detail the IL-dependent phonon self-energies and the e-ph interactions of the combination modes related to the ZA, ZO and ZO′ phonons and (2) we show that the elusive overtone phonon mode 2ZO $q \approx 2k$ is indeed Raman active and its phonon dispersion crosses the LOZO′ combination mode at two different energies, one at about 2.58 eV and another at about 2.78 eV.

Results

Interlayer-related E_L-dependent analysis. Figure 1a shows the phonon combination modes and overtones observed in 2LG in the spectral range 1600 to 1800 cm^{-1}. The insets give the phonon vibration symmetries together with their respective E_L-dependent frequency dispersions for the LOZA (P1) and the two LOZO′ (P2) peaks (upper box in Fig. 1a), and the two 2ZO (P3) peaks (lower box in Fig. 1a). As regards the dispersion relations and phonon peak assignments, our findings for the LOZA and LOZO′ combination modes agree well with those reported in Ref. 8. The LOZA mode (P1 peak in Fig. 1a) comes from a $q \approx 2k$ intravalley phonon scattering process ($q \approx 2k$ AV) showing a frequency dispersion $\partial\omega_{LOZA}/\partial E_L =$ 26.1 cm^{-1}/eV. By looking at the feature P2 in Fig. 1a, we observe that the LOZO′ mode ($q \approx 2k$ AV process) splits into two peaks, LOZO′ (+) and LOZO′(−), whose frequency dispersions are $\partial\omega_{LOZO'(+)}/\partial E_L =$ 55.1 cm^{-1}/eV and $\partial\omega_{LOZO'(-)}/\partial E_L =$ 34.2 cm^{-1}/eV, respectively. As schematized in Fig. 2c, the two P2 peaks do not arise from the phonon dispersion but rather, they come from different resonant regimes of the LOZO′ combination mode with the two electronic valence bands (π_1 and π_2) and the two electronic conduction bands (π_1^* and π_2^*) of 2LG. In other words, the two peaks, LOZO′(+) and LOZO′(−) observed in the Raman spectra, come from the same phonon combination mode LOZO′ but probed at two different points of its phonon dispersion[8]. Indeed, the LOZO′(+) comes from a resonance process involving the $\pi_1(\pi_1^*)$ bands, while the the LOZO′(−) comes from a resonance process involving the $\pi_2(\pi_2^*)$ bands (a process similar to the well-established double-resonance process explaining the G′(2D)-band in 2LG where the iTO phonon exhibits different resonances with the bilayer electronic dispersion[16]). These resonance conditions (see Fig. 2c) require the phonon momentum **q** for the LOZO′(+) mode to be larger than that for the LOZO′(−) mode ($q_{LOZO'(+)} > q_{LOZO'(-)}$). As a consequence the phonon energies are such that $\hbar\omega_{LOZO'(+)} > \hbar\omega_{LOZO'(-)}$.

Next, we discuss the two 2ZO features. Sato *et al.*[11] predicted through tight-binding calculations (see Fig. 1d) that, in 2LG systems, the 2ZO overtone should be observed for forward ($q \approx 0$) and backward ($q \approx 2k$) AV scattering, where the $q \approx 2k$ mode presents a negative frequency dispersion (for clarity, in Ref. 11, the abbreviations for the phonon modes are as follows: oTO stands for ZO, M stands for 2ZO, while oTA stands for ZA and ZO stands for ZO′).

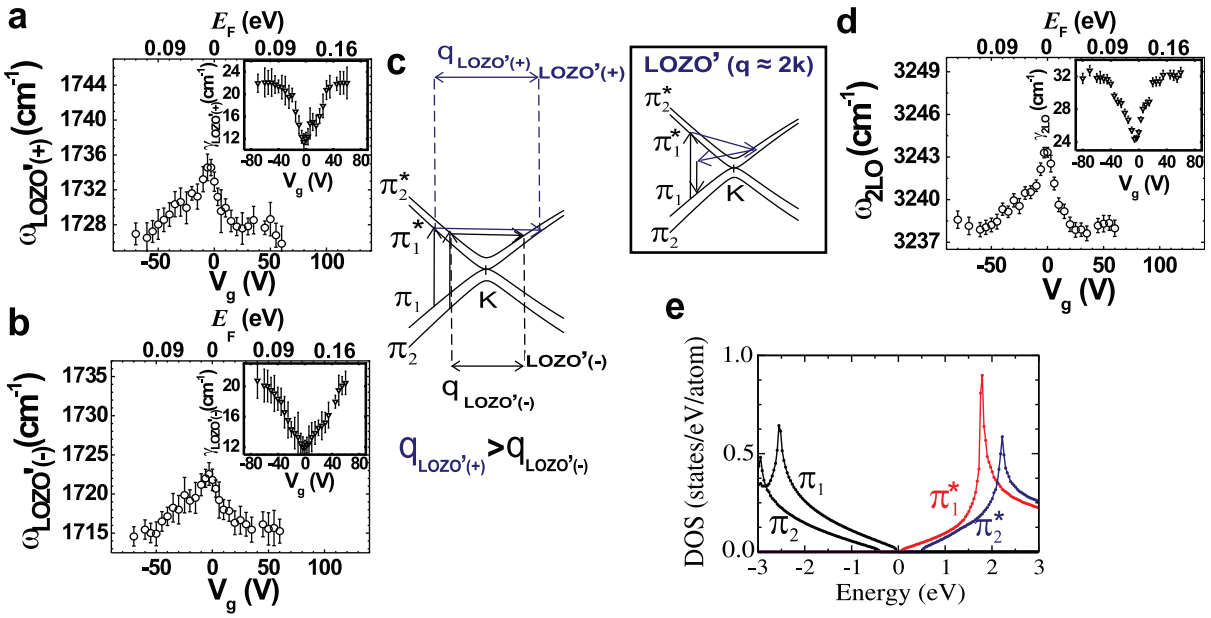

Figure 2 | LOZO′ and 2LO phonon self-energy renormalizations. (a) and (b) show, respectively, the V_g dependence of $\omega_{LOZO'(+)}$ and $\omega_{LOZO'(-)}$. The insets show the V_g dependence of $\gamma_{LOZO'(+)}$ and $\gamma_{LOZO'(-)}$. (c) The LOZO′ mode is resonant with both electronic bands; the $\pi_1(\pi_1^*)$, giving rise to the LOZO′(+) resonance and the $\pi_2(\pi_2^*)$ giving rise to the LOZO′(−) resonance. Note that $q_{LOZO'(+)} > q_{LOZO'(-)}$ implying that $\hbar\omega_{LOZO'(+)} > \hbar\omega_{LOZO'(-)}$. (d) The V_g dependence of ω_{2LO}. The inset shows the V_g dependence of γ_{2LO}. (e) Density of electronic states of 2LG for the valence bands π_1 and π_2(black curves) and for the conduction bands π_1^*(red curve) and π_2^*(blue curve). In (a), (b) and (d) the E_F is related to V_g by $E_F = \mp\gamma_1/2 \pm (1/2)\sqrt{(3\pi a^2\gamma_0^2 C_g)|V_g - V_0|/e + \gamma_1^2}$, where $\gamma_0 \approx 3$ eV is the intralayer carbon atoms hopping, $\gamma_1 \approx 0.4$ eV is the interlayer carbon atoms hopping, $a = 2.46$Å is the lattice constant, $C_g = 1.15 \times 10^{-8}$ F/cm^2 is the geometric capacitance of the system, and V_0 is the gate voltage corresponding to the charge neutrality point, which is monitored by the V_g dependence of the G band frequency.

These authors also predicted that the 2ZO ($q \approx 2k$) would cross the LOZO′ dispersion at $E_L = 2.6$ eV (Fig. 1d). Although some information for the 2ZO ($q \approx 0$) mode was reported by C. H. Lui *et al.*[8], the existence of the 2ZO ($q \approx 2k$) mode remained elusive. Here, as shown in Fig. 1c, we report the 2ZO ($q \approx 2k$) mode which was found to show a negative frequency dispersion $\partial\omega_{2ZO(q\approx 2k)}/\partial E_L = -48.1$ cm^{-1}/eV. Surprisingly, as indicated in Fig. 1c, the 2ZO ($q \approx 2k$) mode crosses the LOZO′(+) at 2.58 eV (predicted in Ref. 11 and is also in good agreement with our observations). However, the 2ZO ($q \approx 2k$) mode has another cross point with the LOZO′(−) mode at 2.78 eV, according to the estimate based on the phonon dispersion observed in the present work. The second crossing at 2.78 eV was not predicted in Ref. 11 and is a consequence of the different dispersions observed for the LOZO′ phonon when this phonon is in resonance with the $\pi_1(\pi_1^*)$ or with the $\pi_2(\pi_2^*)$ bands (only the resonance process with the $\pi_1(\pi_1^*)$ bands was considered by Sato *et al.*[11]). Indeed, these phonon mode crossings could affect both the dynamics of photoexcited carriers and the thermal properties of many systems, since they rely on relaxation processes mediated by high-energy optical and acoustic phonons[17,18]. Recently, it has been shown that the control over the interactions between individual phonon modes and combinations of phonon modes plays an important role in the thermal conductivity of PbTe materials[18]. This is an interesting concept that could be applied to graphene-like materials. It is also important to say that, from Fig. 1c, at higher E_L (4.15 eV according to our observations) the LOZA combination mode might cross the LOZO′ mode too.

Interlayer-related phonon self-energy renormalizations. Having understood the origin of the IL combination of modes and overtones, we next study their phonon self-energy renormalizations, which have not yet been explored. The IL interactions in 2LG rely on the interlayer hopping among equivalent and inequivalent carbon atoms and, therefore, will be directly related to the phonon self-energy and to the e-ph coupling regarding the ZO, ZO′ and ZA modes[3,19]. It is, however, important to note that the LO mode is dependent on the intralayer hopping between two inequivalent carbon atoms, and the LO mode remains essentially unchanged when changing the IL interactions[8–15]. From now on, this manuscript is focused on IL-related phonon self-energy renormalizations. As depicted in the inset of Fig. 2c, the LOZO′ combination mode relates to a $q \approx 2k$ AV process. Note that, Figs. 2a and 2b show, respectively, the E_F dependence of $\omega_{LOZO'(+)}$ and $\omega_{LOZO'(-)}$ when V_g is varied. Both, $\omega_{LOZO'(+)}$ and $\omega_{LOZO'(-)}$ soften with increasing $|E_F|$ which is controlled by increasing $|V_g|$. Correspondingly, as shown in the insets of Figs. 2a and 2b, the phonon line widths $\gamma_{LOZO'(+)}$ and $\gamma_{LOZO'(-)}$ broaden with increasing $|E_F|$. Analogously, Fig. 3a shows that ω_{LOZA} (γ_{LOZA}) softens (broadens) with increasing $|E_F|$, while for the 2ZO overtone, a negligible dependence on V_g is observed for both ω_{2ZO} and γ_{2ZO} (Fig. 3b).

As a reminder, this behavior is opposite to what happens to the $q = 0$ phonons at the Γ-point[20], as is the case of the G-band feature, where $\omega_{\mathbf{q}}$ hardens and $\gamma_{\mathbf{q}}$ narrows when $|E_F|$ increases as a consequence of electron-hole (e-h) pair creation (annihilation) due to phonon absorption (emission). For $q = 0$ phonons at the Γ-point, the e-h pair creation (annihilation) is halted by the Pauli principle, when $2|E_F| > \hbar\omega_q$. As explained by Araujo *et al.* for monolayer graphene[19], for both intravalley AV and intervalley EV $q \neq 0$ phonons, instead of the Pauli principle, the density of electronic and vibrational states together with energy and momentum conservation requirements will be responsible for halting e-h pair production. Indeed, for $|E_F| = 0$ the density of states is almost null and the electronic structure slope ($\partial E(\mathbf{k})/\partial \mathbf{k}$) is larger than the vibrational structure slope ($\partial\omega(\mathbf{q})/\partial\mathbf{q}$) so that no phonon can couple to any electrons[19]. In this case no phonon self-energy renormalization due to e-h pair creation (annihilation) is observed. However, when $|E_F|$ increases, the density of states increases and the difference between the slopes of the electronic and vibrational dispersions decreases[19]. In this situation,

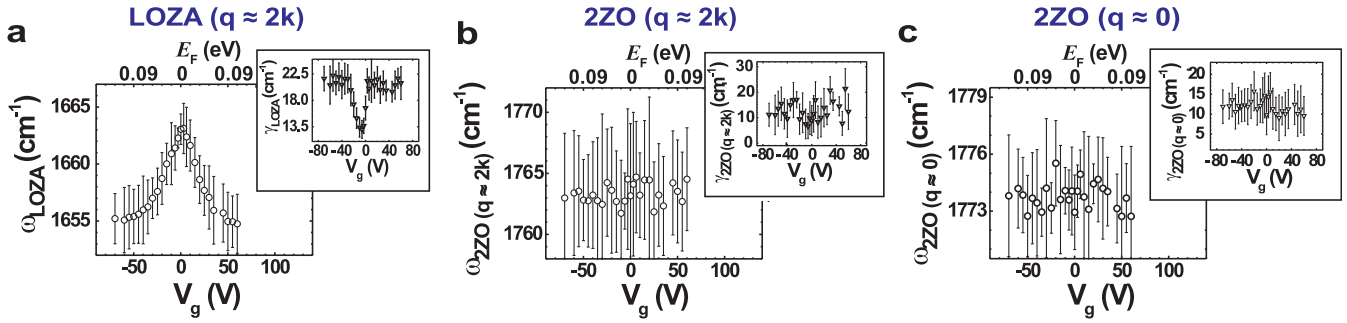

Figure 3 | LOZA and 2ZO phonon self-energy renormalizations. (a) and (b) show, respectively, the V_g dependence of ω_{LOZA}, ω_{2ZO} for the $q \approx 2k$ AV process and (c) shows V_g dependence of ω_{2ZO} for the $q \approx 0$ AV process. The insets show the V_g dependence of the line widths γ_{LOZA}, γ_{2ZO} for the $q \approx 2k$ AV process ((a) and (b), respectively) and γ_{2ZO} for the $q \approx 0$ AV process (c).

phonon self-energy corrections are observed since the density of states is non-null and a phonon with momentum $\mathbf{q}$ can connect two electronic states $\mathbf{k}$ and $\mathbf{k}'$ while fulfilling the energy and momentum requirements. In order to quantify the ZO′ phonon self-energy corrections, we measured the V_g dependence of ω_{2LO} and γ_{2LO} for the 2LO overtone (see Fig. 2d), which is known as the 2D′ band around 3244 cm^{-1}. In analogy to the LOZO′ combination mode about the Γ-point, the 2LO overtone is a $q \approx 2k$ AV double resonant process and is a fruitful choice for unraveling the two-phonon self-energy contributions that are merged in the LOZO′ combination mode.

The Raman scattering process involving overtone or combinations of phonon modes will conserve both the frequency and momentum, so that in our case (for the Stokes process) $\omega_s = \omega_L - (\omega_{LO} + \omega_j)$ and $\mathbf{k}_s = \mathbf{k}_L - (\mathbf{q}_{LO} + \mathbf{q}_j)$, where $\omega_s(\mathbf{k}_s)$ is the frequency (momentum) of the Stokes scattered light, $\omega_L(\mathbf{k}_L)$ is the frequency (momentum) of the incident light, $\omega_{LO}(\mathbf{q}_{LO})$ is the frequency (momentum) of the LO phonon mode and $\omega_j(\mathbf{q}_j)$ is the frequency (momentum) of the ZO, ZO′ or ZA phonon modes. Since the electron is vertically excited from the valence to the conduction band by the absorption of a photon, we have $\mathbf{k}_s = \mathbf{k}_L$ and, therefore, the phonon momenta will be such that $\mathbf{q}_{LO} \approx \mathbf{q}_j$. This scattering process is understood as follows: the electron is first scattered by one of the phonons, let us say the LO phonon, and then the electron is scattered again by a second phonon; LO, if an overtone is observed or ZO, ZO′ and ZA if a combination mode is observed. On top of this, the phonon self-energy renormalization relies on each specific phonon mode, being described by[21]:

$$\Pi(\omega_q, E_F) = 2\sum_{kk'} \frac{|V_{kk'}|^2}{\hbar\omega_q - E^{eh} + i\gamma_q/2} \times (f_h - f_e) \qquad (1)$$

where $\mathbf{k}$ and $\mathbf{k}'$ are, respectively, wave-vectors for the initial and final electronic states; $\mathbf{q} \equiv \mathbf{k} - \mathbf{k}'$ is the phonon wave-vector; $E^{eh} \equiv \left(E^e_{k'} - E^h_k\right)$ is the e-h pair energy; $\omega_\mathbf{q}$ is the phonon frequency; $\gamma_\mathbf{q}$ is the phonon linewidth; $f_h(f_e)$ is the Fermi distribution function for holes (electrons) and $V_{kk'}$ gives the el-ph coupling matrix element. The renormalization will happen independently for each phonon, so that, as a first approximation for a combination mode or overtone, the renormalization will be $\Pi(\omega_{LO+j}, E_F) = \Pi(\omega_{LO}, E_F) + \Pi(\omega_j, E_F)$, where j is a LO mode if an overtone is considered or j is a ZO, ZO′ and ZA if a combination mode is considered. Moreover, the IL interactions governing the ZO, ZO′ and ZA modes will not change the intralayer dependent LO mode[8–11]. Therefore, what we are observing in the gate-modulated Raman experiment for overtone and phonon combination modes is, indeed, the summation of the individual phonon self-energy corrections of each phonon participating of the scattering process[21]. The phonon self-energy renormalization strengths will be quantified by the difference between the frequencies ω^0_q at $V_g = 0$ and $\omega_\mathbf{q}$ for $V_g \neq 0$, *i.e.*, $\Delta\omega_q = \mathrm{Re}\left[\Pi(\omega_q, E_F)\right] = \omega_q - \omega^0_q$ (the renormalization strength could also be obtained from the phonon linewidth, which will be reported elsewhere), which is the real part of equation 1. As explained above, ω^0_q at $V_g = 0$ describes the system with no renormalizations that are associated with electron-hole (e-h) pair formation.

Discussion

By inspecting Figs. 2a and 2b, we find that $\Delta\omega_{LOZO'(+)} = 9$ cm^{-1} and $\Delta\omega_{LOZO'(-)} = 7$ cm^{-1}, respectively. On the other hand, by looking at Fig. 2d we see that $\Delta\omega_{2LO} = 5$ cm^{-1}, which means that the LO frequency renormalization for this AV process is $\Delta\omega_{LO} \approx 2.5$ cm^{-1}. The self-energy corrections regarding the LO mode will be the same for the LO contribution for both the LOZO′(+) and LOZO′(−) features. Therefore the phonon self-energy correction $\Delta\omega_{ZO'(+)}$ for the ZO′(+) mode will be given by $\Delta\omega_{LOZO'(+)} - \Delta\omega_{LO} = 6.5$ cm^{-1} while the phonon self-energy correction $\Delta\omega_{ZO'(-)}$ for the ZO′(−) mode will be given by $\Delta\omega_{LOZO'(-)} - \Delta\omega_{LO} = 4.5$ cm^{-1}. From the analysis above and remembering that, the larger the self-energy corrections $\Delta\omega_\mathbf{q}$, the stronger are the e-ph couplings, we deduce that the IL e-ph coupling mediating the renormalizations for the ZO′ mode is stronger than the renormalization for the LO mode. It is noteworthy that the self-energy renormalizations for LOZO′(+) and LOZO′(−) are different even though they involve the same LO phonon. We understand these differences as follows: the phonon self-energy corrections for $q \neq 0$ phonons rely on the density of electron and phonon states[19]. The density of phonons states will be the same because the same phonon is involved. However, as shown in Fig. 2e, for energies smaller than |2| eV, the density of electronic states for $\pi_2(\pi^*_2)$ is always smaller than that for $\pi_1(\pi^*_1)$. This means that the phonon self-energy corrections are weaker for the ZO′(−) in comparison to that for the ZO′(+) not due to a different e-ph coupling symmetry, but because the density of electronic states for $\pi_2(\pi^*_2)$ is smaller in comparison to that for $\pi_1(\pi^*_1)$, as seen in Fig. 2e. By following the same strategy, we could also estimate the phonon self-energy corrections for the ZA mode, whose LOZA combination mode frequency (linewidth) also hardens (broadens) as expected for $q \neq 0$ AV processes. As shown in Fig. 3a, $\Delta\omega_{LOZA} = 8$ cm^{-1}. Therefore, the ZA mode self-energy corrections $\Delta\omega_{ZA}$ will be given by $\Delta\omega_{LOZA} - \Delta\omega_{LO} = 5.5$ cm^{-1}. It is interesting to note that, the renormalization for the ZA mode is similar to that ruling the ZO′ mode. Moreover, we note that this is the first time the phonon self-energy renormalizations of an acoustic mode are reported.

Next, we discuss the V_g dependence of the 2ZO overtone for both, $q \approx 0$ and $q \approx 2k$ AV processes. Interestingly, the results in Figs. 3b and 3c show that, for both cases, the phonon self-energy corrections to the phonon frequency $\Delta\omega_{2ZO}$ and to the line width $\Delta\gamma_{2ZO}$, are weak and as a consequence, the ω_{2ZO} and γ_{2ZO} renormalizations show a constant behavior with increasing $|E_F|$. This result is

understood as follows: for phonon self-energy corrections, the phonon energies themselves will determine where in the Dirac cones the e-h pair creation (annihilation) will be happening and, therefore, will determine the initial (final) density of electronic and vibrational states. On top of this, the momentum conservation requirement $\mathbf{q} = \mathbf{k} - \mathbf{k}'$, which is mostly determined by the slopes in the electronic and vibrational dispersion relations, must be obeyed in order to observe a strong coupling. Comparing all the cases, the ZO phonon mode would create (annihilate) an e-h pair at much higher energies $\sim$ 110 meV and, therefore, at a much higher density of electronic and vibrational states compared to the energies of the ZA ($\sim$ 3.1 meV) and the ZO′ ($\sim$ 11.2 meV) modes. Because phonon renormalizations can be observed for both the ZA and ZO′ modes, the authors understand that the reason behind the weak renormalization observed for the ZO mode is due to the lack of a phonon momentum $\mathbf{q}$ such that $\mathbf{q} = \mathbf{k} - \mathbf{k}'$, and this lack prevents any resonant renormalization from happening. This is confirmed by symmetry arguments since the deformation potential mediating the e-ph coupling related to the ZO mode, which is an anti-symmetric IL vibration, is not expected to allow coupling of orthogonal electronic states since its vibration breaks the lattice symmetry, which implies $V_{\mathbf{kk}'} = 0$ in equation 1. Thus, no renormalizations are expected for the 2ZO mode[22].

It is worth commenting that 1LG and 2LG are essentially different as regards the electronic structure but very similar as regards the vibrational structure (except for the LBM). Nevertheless, the phonon renormalization phenomena happen similarly in 1LG and 2LG for AV $q \neq 0$ processes where $\omega_{\mathbf{q}}$ ($\gamma_{\mathbf{q}}$) softens (broadens) with increasing $|V_g|$. This is interesting since under the application of V_g, 1LG still remains a zero-gap material around the **K**-point with massless carriers, contrary to the case of 2LG, in which a band-gap is opened when there is an asymmetry between the two layers. Another point is that 2LG presents a new scenario where the symmetry of the vibration is important to determine whether or not the e-ph coupling renormalizations will take place, which was not the case for 1LG (since the ZO mode is Raman-inactive in 1LG).

Finally, the micro-mechanical cleavage of bulk graphite (so-called Scotch-tape method) gives 2LG graphene samples with mostly AB-stacked structures and the strongest IL interactions. For this reason, the 2LG system obtained from exfoliation is the best system to provide the fundamental physics behind the IL related phonon self-energy renormalizations. Another commonly used synthesis method is the Chemical Vapor Deposition (CVD). Through the CVD method, in general, the 2LG system is grown in two steps where in step one a graphene layer is grown and in step two, the second graphene layer is epitaxially deposited over the first. Recently, selected area electron diffraction (SAED) and Raman scattering have been used to show that the resultant 2LG systems grown by the CVD methods are AB-stacked[23,24]. Indeed, the Raman G′(2D)/G intensity ratio ($\approx$ 1) for the CVD grown 2LG system agrees well with the Scotch-tape sample and also the G′-band linewidth ($\approx$ 60 cm^{-1}) is similar. In fact, the lineshape for the G′ band can be interpreted in terms of four peaks whose frequencies (ranging from 2640 to 2715 cm^{-1}) and linewidths ($\approx$ 30 cm^{-1}) are basically the same as the ones found for the Scotch-tape sample. However, the G′ lineshape, which is determined by the Raman cross-sections of each of the four peaks, is slightly different mainly because the little shoulder around 2645 cm^{-1} observed for the Scotch-tape samples[16] is not evident in the CVD grown samples. This shows that the interlayer interactions are quite similar for both production methods but not exactly the same and further studies are clearly needed to explain these small differences in detail. It is important to say that, although some similarities are expected between different methods of producing 2LG samples, these different methods will produce 2LG samples with IL interactions which are different. However, it is noteworthy that the phonon behavior in which $\omega_{\mathbf{q}}$ ($\gamma_{\mathbf{q}}$) softens (broadens) with increasing $|V_g|$ is related to the fact that the phonon wave vector is different of zero ($q \neq 0$). This phenomenon is explained in detail by the authors in a previous publication[20].

The magnitude of the IL interactions can strengthen/weaken the phonon self-energy renormalizations since the electron-phonon coupling mediating these renormalizations relies on the IL interactions magnitude. Indeed, our results are obtained from exfoliated samples which means a perfect stacking between the two layers forming the 2LG system but we still cannot assert how the results of this work will apply for small angles. However, as explained by Kim *et al.*[25], when the orientation in between the two layers in a turbostratic 2LG is higher than a certain critical angle (around 13°), the two graphene layers behave as if they are independent from each other. This means that the interlayer interaction at that point is negligible and no interlayer related modes are supposed to appear. For angles smaller than the critical angle, where there are some meaningful interactions, we expect to observe the interlayer related modes whose spectral features will depend on the stacking angle. For different coupling magnitudes between the top and the bottom layer, we should find different magnitudes for the phonon self-energy renormalizations, which will be smaller if the interlayer interaction is likewise smaller.

Methods

The E_L-dependent measurements were done in the back scattering configuration using E_L values ranging from 2.10 to 2.54 eV with a 100× objective. The laser power was kept around 1.5 mW to avoid heating effects on our graphene samples. The samples were produced by the micro-mechanical cleavage of graphite on a Si substrate covered with 300 nm of SiO_2. The gate-dependent measurements were performed with the 2.33 eV laser in devices fabricated by lift-off patterning of thermally evaporated Cr/Au (5 nm/80 nm, respectively). Back gate measurements were done near 300 K with voltages ranging from −70 to 70 V (Fermi level variation $|E_F| \approx 150$ meV). The E_F is related to V_g by $E_F = \mp\gamma_1/2 \pm (1/2)\sqrt{(3\pi a^2\gamma_0^2 C_g)|V_g - V_0|/e + \gamma_1^2}$, where $\gamma_0 \approx$ 3 eV is the intralayer carbon atoms hopping, $\gamma_1 \approx 0.4$ eV is the interlayer carbon atoms hopping, $a = 2.46$Å is the lattice constant, $C_g = 1.15 \times 10^{-8}$ F/cm^2 is the geometric capacitance of the system and V_0 is the gate voltage corresponding to the charge neutrality point, which is monitored by the V_g dependence of the G band frequency.

1. Bostwick, A., Ohta, T., Seyller, T., Horn, K. & Rotenberg, E. Quasiparticle dynamics in graphene. *Nat. Phys.* **3**, 36–40 (2007).
2. Park Cheol, H., Giustino, F., Cohen, M. L. & Louie, S. G. Electron-phonon interactions in graphene, bilayer graphene, and graphite. *Nano Lett.* **8**, 4229–4233 (2008).
3. Castro Neto, A. H. *et al.* The electronic properties of graphene. *Rev. Mod. Phys.* **81**, 109–162 (2009).
4. Ma, R. & Sasaki, T. Nanosheets of oxides and hydroxides: ultimate 2D charge-bearing functional crystallites. *Adv. Mater.* **22**, 5082–5104 (2010).
5. Schwierz, F. Graphene transistors. *Nat. Nanotech.* **5**, 487–496 (2010).
6. Lemme, M. C. *et al.* Gate-activated photoresponse in a graphene p-n junction. *Nano Lett.* **11**, 4134–4137 (2011).
7. Lui, C. H., Li, Z., Mak, K. F., Cappelluti, E. & Heinz, T. F. Observation of an electrically tunable band gap in trilayer graphene. *Nat. Phys.* **7**, 944–947 (2011).
8. Lui, C. H., Malard, L. M., Kim, S., Lantz, G., Laverge, F. E., Saito, R. & Heinz, T. F. Observation of out-of-plane vibrations in few-layer graphene. *Nano Lett.* **12**, 5539–5544 (2012).
9. Zhang, L. M. *et al.* Raman and infrared properties and layer dependence of the phonon dispersions in multilayered graphene. *Phys. Rev.* B **78**, 235408 (2008).
10. Kuzmenko, A. B. *et al.* Determination of the gate-tunable band gap and tight-binding parameters in bilayer graphene using infrared spectroscopy. *Phys. Rev. B* **80**, 165406 (2009).
11. Sato, K. *et al.* Raman spectra of out-of-plane phonons in bilayer graphene. *Phys. Rev. B* **84**, 035419 (2011).
12. Kitipornchai, S., He, X. Q. & Liew, K. M. Continuum model for the vibration of multilayered graphene sheets. *Phys. Rev. B* **72**, 075443 (2005).
13. Saha Srijan, K., Waghmare, U. V., Krishnamurthy, H. R. & Sood, A. K. Phonons in few-layer graphene and interplanar interaction: A first-principles study. *Phys. Rev. B* **78**, 165421 (2008).
14. Yan Jia, A., Ruan, W. Y. & Chou, M. Y. Phonon dispersions and vibrational properties of monolayer, bilayer, and trilayer graphene: Density-functional perturbation theory. *Phys. Rev. B* **77**, 125401 (2008).
15. Jiang Jin, W., Tang, H., Wang Bing, S. & Su Zhao, B. Raman and infrared properties and layer dependence of the phonon dispersions in multilayered graphene. *Phys. Rev. B* **77**, 235421 (2008).

16. Malard, L. M., Pimenta, M. A., Dresselhaus, G. & Dresselhaus, M. S. Raman spectroscopy in graphene. *Phys. Rep.* **473**, 51–87 (2009).
17. Echtermeyer, T. J. *et al.* Strong plasmonic enhancement of photovoltage in graphene. *Nat. Commun.* **2**, 458 (2011).
18. Delaire, O. *et al.* Giant anharmonic phonon scattering in PbTe. *Nat. Mater.* **10**, 614–619 (2011).
19. Malard, L. M. *et al.* Probing the electronic structure of bilayer graphene by Raman scattering. *Phys. Rev. B* **76**, 201401(R) (2007).
20. Araujo, P. T., Mafra, D. L., Kong, J., Sato, K., Saito, R. & Dresselhaus, M. S. Phonon self-energy corrections to nonzero wave-vector phonon modes in single-layer graphene. *Phys. Rev. Lett.* **109**, 046801 (2012).
21. Taylor, P. L. & Heinonen, O. *A quantum approach to condensed matter physics.* (University Press Cambridge, United Kingdom, 2004).
22. Chakraborty, B. *et al.* Symmetry-dependent phonon renormalization in monolayer MoS2 transistor. *Phys. Rev. B* **85**, 161403(R) (2012).
23. Wu, Y. *et al.* Growth mechanism and controlled synthesis of AB-stacked bilayer graphene on Cu-Ni alloy foils. *ACS Nano* **6**, 7731–7738 (2012).
24. Liu, L. *et al.* High-yield chemical vapor deposition growth of high-quality large-area AB-stacked bilayer graphene. *ACS Nano* **6**, 8241–8249 (2012).
25. Kim, K. *et al.* Raman spectroscopy study of rotated double-layer graphene: misorientation-angle dependence of electronic structure. *Phys. Rev. Lett.* **108**, 246103 (2012).

Acknowledgments

P.T.A. acknowledges ONR-MURI-N00014-09-1-1063 and J.F. Rodriguez-Nieva for helpful discussions. D.L.M. acknowledges CNPq-Brazil financial support. R.S. and K.S. acknowledge MEXT grant No.20241023 and No.23710118, respectively. M.S.D. and J.K. acknowledge NSF-DMR 10-04147 and 08-45358, respectively.

Authors contributions

P.T.A. and D.L.M. designed the experiments, performed the measurements and analyzed the experimental data. All the authors discussed the results and wrote the manuscript.

Additional information

Competing financial interests: The authors declare no competing financial interests.

How to cite this article: Araujo, P.T. *et al.* Unraveling the interlayer-related phonon self-energy renormalization in bilayer graphene. *Sci. Rep.* **2**, 1017; DOI:10.1038/srep01017 (2012).